

HIGH RESOLUTION MEASUREMENT OF THE $K\alpha$ SPECTRUM OF Fe XXV–XXVIII: NEW SPECTRAL DIAGNOSTICS OF NONEQUILIBRIUM ASTROPHYSICAL PLASMAS

V. DECAUX¹ AND P. BEIERSDORFER

Lawrence Livermore National Laboratory, University of California, Livermore, CA 94551

S. M. KAHN²

Departments of Physics and Astronomy and Space Sciences Laboratory, University of California, Berkeley, CA 94720

AND

V. L. JACOBS

Complex Systems Theory Branch, Code 6693, Condensed Matter and Radiation Sciences Division,
Naval Research Laboratory, Washington, DC 20375-5345

Received 1996 July 5; accepted 1997 January 2

ABSTRACT

We present laboratory measurements of high-resolution spectra of iron $K\alpha$ emission under transient ionization conditions similar to those that are believed to exist in stellar flares and young supernova remnants. Taking advantage of our high spectral resolution ($\lambda/\Delta\lambda \geq 2000$), we identify a number of transitions that can serve as diagnostics of ionizing plasmas. By varying the excitation energy in the experiments, we constrain the effects of the electron distribution on these diagnostic lines. Using our measured line ratios, we deduce values for the ionization time, $\eta = N_e t$, in the plasma, which agree with the actual values to $\sim 20\%$ accuracy. This result gives us confidence to our ability to derive similar constraints on astrophysical plasmas from remote X-ray spectroscopic observations.

Subject headings: atomic data — atomic processes — methods: laboratory — plasmas

1. INTRODUCTION

Because of iron's relatively large abundance among intermediate- Z elements, X-ray transitions of iron are of great importance to cosmic X-ray spectroscopy (see Treves, Perola, & Stella 1991; Silver & Kahn 1993). Of particular interest are the K-shell transitions, which, with energies in the 6.4–6.9 keV energy range, are well separated from other X-ray features. While the spectra recorded to date have proven that iron K lines are emitted by a wide variety of cosmic sources, upcoming dramatic improvements in instrument resolution and sensitivity are expected to allow for a more precise identification of the individual contributing charge states and a more detailed understanding of the fundamental radiative emission processes in these plasmas. For instance, spectral resolving powers on the order of 670 at 6.7 keV are expected for the X-Ray Spectrometer (XRS) microcalorimeter experiment that will be flown on the upcoming *Astro-E* mission (Kelley 1996, private communication).

While most studies of the X-ray spectra of iron have been concerned with plasmas under steady-state conditions, such as stellar coronae, it has been suggested that transient ionization conditions can also play an important role in astrophysical plasmas, as in the shock-front-heated regions of young supernova remnants (e.g., Itoh 1977, 1978; Shapiro & Moore 1976) or impulsively heated gas in solar flares (e.g., Kafatos & Tucker 1972; Mewe & Schrijver 1975, 1978, 1980; Shapiro & Moore 1977; Shapiro & Knight 1978). For these cases the establishment of ionization balance lags behind a sudden increase in electron temperature, which dramatically affects the emitted X-ray spectra. After integra-

tion over time, $K\alpha$ emission from all existing charge states of iron (Fe I–XXVI) can be observed. This result stands in sharp contrast to the more traditional situation found in plasmas for which collisional ionization equilibrium has been established, in which the $K\alpha$ spectrum is dominated by the emission from Fe XXV and Fe XXVI because K-shell transitions cannot be excited at the lower electron temperatures where less ionized species are prevalent. Also, while dielectronic recombination (DR) is usually the dominant line formation process in equilibrium plasmas with a Maxwellian electron distribution (see Beiersdorfer et al. 1993b), this process plays an insignificant role in ionizing plasmas.

In this paper, we present a laboratory simulation of X-ray line formation under transient ionization conditions using the Livermore Electron Beam Ion Trap (EBIT). The electron density in the EBIT is similar to the electron density of solar flares, which is on the order of 10^{11} – 10^{12} cm^{-3} . Since our spectral resolution ($\lambda/\Delta\lambda \geq 2000$) exceeds that of present and near-future satellite facilities (the resolution of EBIT is about three times better than that of *Astro-E*), our measurements are well suited to serve as benchmarks for detailed models of transient ionization, which have not previously been tested to this level of accuracy. Such models are inherently complex: a large number of inner-shell excited emission lines in the $K\alpha$ spectra, from all ionization stages of iron, especially Fe XVIII through Fe XXV, must be taken into account, including the rates for radiative decay, inner-shell excitation, inner-shell ionization, and autoionization. In fact, some of the spectral lines involved in the atomic models have only recently been identified in observations (Beiersdorfer et al. 1993b; Decaux & Beiersdorfer 1993; Decaux et al. 1995).

Our experiment involved measuring the transient spectral structure as a function of time in the wavelength range 1.84–1.94 Å, which includes the $K\alpha$ emission features of all charge states from Fe XXV down to Fe I. In the present work

¹ Present address: PRIMEX Physics International, 2700 Merced Street, San Leandro, CA 94577.

² Present address: Department of Physics and Columbia Astrophysics Laboratory, Columbia University, 538 W 120th Street, New York, NY 10027.

the focus has been on the intermediate charge states Fe xviii–xxv, which are well resolved in our spectra. We have utilized for these charge states a modified version of the detailed $K\alpha$ spectral model developed by Jacobs et al. (1989). Transient spectra of Fe x–xviii have been presented in a previous paper (Decaux et al. 1995). Our measurements provide the first experimental validation of the theoretical predictions of Mewe & Schrijver (1980). While good overall agreement with these predictions is found, there are some discrepancies, most notably in Fe xx, which we discuss below. Because the $K\alpha$ spectra are emitted under conditions that are far removed from collisional ionization equilibrium, we observe, during the early stages of the ionization process, an enhanced low- to high-charge-state ratio for the X-ray features. A clear signature of the enhanced ratio is the identification of Fe xviii–xxii emission features in the spectra, as well as an unresolved structure around 1.93 Å in the early-time spectrum containing contributions from all charge states below Fe xviii (Decaux et al. 1995). Another characteristic of the nonequilibrium ionization conditions is the increased importance of lines resulting from K-shell ionization when the excitation energy exceeds the threshold energy for the ionization process. Indeed, the detection of such lines might provide a diagnostic of the presence of a nonthermal high-energy tail in the electron distribution. These hard tails on the electron distribution are expected to occur in a number of diverse astronomical environments in which ionizing plasmas are encountered. In particular, in young supernova remnants, first-order Fermi acceleration at the shock front can produce nonthermal electrons with an essentially power-law spectrum extending from energies of order of a few keV to several MeV. In solar and stellar flares, sudden energy release mechanisms, such as magnetic reconnection, that are believed to “power” the flares, not only heat the thermal plasmas confined in magnetic loops, but also produce nonthermal particles that are directed back into the photosphere or out into interstellar space. In both cases, diagnostics of such nonthermal particle populations are crucial for constraining the value of the total energy in the emitting plasmas and for understanding the nature of the transient heating. In the past, the presence of hard tails in electron distributions has only been deduced from the shape of the X-ray continuum, i.e., departure from the bremsstrahlung spectrum expected for a purely thermal plasma. However, this is a subtle effect that is difficult to measure in most cases, and the use of iron K-shell line ratios may be far more promising. Since inner-shell ionization requires electrons with energies above the K edge, line ratios that are sensitive to this process provide a clean constraint on the higher energy electron population.

We find that the observed spectroscopic features are well represented by the theoretical calculations. In particular, the line ratios of the features within each charge state are reproduced with good accuracy. This result is of particular significance for the charge states Fe xviii–xxi, which we use to deduce from our spectroscopic data the ionization time $\eta = N_e t$, where N_e is the electron density and t is the time measured from the beginning of the ionization process. This quantity is of fundamental importance and is the principal parameter used to characterize ionizing plasmas. In the case of supernova remnants, where the time since the explosion is known, the value of the density N_e can be inferred if the parameter η is determined spectroscopically.

As a result of the good agreement between the experimental and theoretical results for spectral line ratios within each charge state, we were able to reproduce accurately the experimental data by adjusting only the charge-state population fractions. For the case of the charge states Fe xvii–xxi, the result of this fit to the experimental data was compared to the result of a theoretical time-dependent charge-state balance model. By adjusting the electron density in this model, we were able to determine the value of N_e for which the model result is in agreement with the experimentally determined charge-state population fractions. Since the value of the time parameter was set by our experiment, we can provide a direct correlation between the observed data and the ionization time. We show that this correlation can be given to an accuracy of $\sim 20\%$.

This paper is organized as follows. In § 2, we describe the EBIT and review our experimental procedure. In § 3, we present our measured spectra and compare them to published predicted spectra for ionizing plasmas. In § 4, we discuss the effects of K-shell ionization and the consequent spectral dependence on the shape of the electron distribution. Since many spectral features associated with the lower charge states are blended, we have relied on model calculations incorporating all relevant atomic excitation processes to identify the features. By comparing the experimental spectra with the predictions from a detailed time-dependent model, we demonstrate in § 5 that spectral data can be used to quantitatively determine the relative charge-state population fractions as functions of time, which can be used to deduce the ionization time η with good accuracy. Finally, our conclusions are presented in § 6.

2. EXPERIMENTAL PROCEDURE

The K-shell X-ray lines originating from charge states lower than Fe xxiv are very difficult to observe in plasmas in ionization equilibrium with a Maxwellian electron energy distribution, partly because the energy necessary for the excitation of the $K\alpha$ lines (6.4 keV for iron) is substantially higher than the threshold energy associated with the ionization of an ion to the heliumlike charge state (2.05 keV for iron). In addition, the K-shell excitation processes in ionizing plasmas have cross sections on the order of only a few $\times 10^{-22}$ cm². By contrast, ionization of L- and M-shell electrons, leading to the destruction of a given charge state, is much more likely, with cross sections of about 5×10^{-20} cm² and $(0.44\text{--}1.1) \times 10^{-18}$ cm², respectively. Thus, $K\alpha$ transitions from lower charge states are expected to be prominent only during nonequilibrium or transient ionization conditions. This result is especially apparent for the lowest charge states of iron, such as those below Fe xviii. Consequently, the observation of $K\alpha$ lines from these lower charge states can be used for the identification and investigation of nonequilibrium ionization conditions, such as the ionizing-plasma conditions that are characteristic of young supernova remnants (Decaux et al. 1995).

As we will point out later in § 4, the rate coefficients for both K-shell ionization and collisional excitation are of comparable magnitude and on the order of 10^{-12} cm³ s⁻¹, which is a relatively low value. As a result, the K-shell lines are not very bright and highly sensitive measuring instruments must be used in the future to make such observations in the astrophysical medium.

We simulated the transient conditions necessary for the observation of these lower charge states in the laboratory using the Livermore Electron Beam Ion Trap (EBIT). Detailed descriptions of this device are given by Levine et al. (1988) and by Marrs et al. (1988). The EBIT consists of an electron beam that is initiated by a Pierce-type electron gun and compressed to a radius of $\sim 30 \mu\text{m}$ in a 3 T magnetic field generated by a pair of superconducting Helmholtz coils. The layout of the EBIT is shown in Figure 1. The space charge of the electron beam confines the ions, and collisions with the beam electrons both ionize the trapped ions and excite X-ray transitions in them. Compared to other X-ray sources, the EBIT device provides the unique advantage of allowing the selection of a particular atomic excitation mechanism in any given ion (Beiersdorfer et al. 1993a). This selection can be achieved by tuning the nearly monoenergetic electron beam (which has an energy spread $\approx 50 \text{ eV}$ FWHM). Moreover, the EBIT is ideally suited for high-precision spectroscopy, because the emitting ions are stationary and the observed X-ray lines are free of any Doppler shifts. Since EBIT was originally designed as an X-ray source, six radial ports are provided, which allow for the observation of the spectra emitted by the trapped ions in a plane perpendicular to the electron beam. The measurements presented in this paper were carried out using a high-resolution crystal spectrometer in the von Hámos configuration (von Hámos 1933; Beiersdorfer et al. 1990). The EBIT conditions for these experiments were as follows: beam current $I_{\text{beam}} = 150 \text{ mA}$, ion density $N_i \approx 10^9 \text{ cm}^{-3}$, and current density $J \approx 5300 \text{ A cm}^{-2}$.

Singly or doubled charged iron ions were produced by a metal vapor vacuum arc (MeVVA; Brown et al. 1986) and injected into the EBIT at time $t = 0 \text{ s}$, at which time the interaction with the electron beam commenced. Then a series of 15 spectra was recorded sequentially during the ionization process. The timescale for the production of

Fe xxv was less than 1 s, and it was as short as a few ms for the charge states below Fe xxi. After recording the 15 spectra, the ions were removed from the trap and the process was repeated many times over a period of several hours. The procedure was similar to that described previously by Decaux & Beiersdorfer (1993). We recorded the K-shell emission at two different electron beam energies, above and below the K-shell ionization threshold at 6.9 and 12.0 keV, respectively. For these measurements, the time resolution was 20 ms. A third measurement was performed, also at 12 keV, with a time resolution of 7 ms, in order to characterize with greater precision the early-time evolution of the population fractions for the intermediate charge states (Fe xviii–xxi).

3. COMPARISON TO MODEL IONIZING SPECTRA

Results of the first two measurements are shown in Figure 2 (corresponding to a beam energy of 12.0 keV) and Figure 3 (corresponding to a beam energy of 6.9 keV). The iron $K\alpha$ emission in Figure 2 includes the contributions from all eight charge states of Fe xviii through Fe xxv in the wavelength region between 1.85 and 1.94 Å. Individual features are labeled using the notation of Table 1. The wavelength scale was established using known reference lines and is accurate to within 0.3–0.5 mÅ. The measured spectra illustrate the characteristic behavior of the sequential ionization process: for the earliest phase of the ionization process, 0–20 ms after injection, the spectrum mainly shows emission from the intermediate ions Fe xviii–xx, while the emission from the higher ions Fe xxii–xxv is found to be dominant at later stages.

The experimental spectrum presented in Figure 2 shows agreement with the theoretical predictions for shock-excited astrophysical plasmas obtained by Mewe & Schrijver (1980). Particularly good agreement is obtained with the theoretical model referred to as model A, the “impulsive burst” model, for which a temperature jump occurs at $t = 0$, the temperature increasing from an initial value $5 \times 10^6 \text{ K}$ to a constant final value of $50 \times 10^6 \text{ K}$ for $N_e = 10^{10} \text{ cm}^{-3}$. The measured spectra for the 0–20, 40–60, and 80–100 ms intervals show good agreement with the calculated spectra for $t = 0.1, 6, \text{ and } 10 \text{ s}$ after the passage of the shock front. There are, however, some differences, particularly for Fe xx, where this model predicts that the two principal features (N5 and N11) are dominant in the spectra at $t = 1 \text{ s}$ and $t = 2 \text{ s}$. By contrast, these lines are never very pronounced in our experimental data. Conversely, this model shows that the complex B4 + B5 in Fe xxii should be quite weak, in particular relative to line β (or E3) in Fe xxiii; this prediction is not found to be in agreement with our experimental data. We also point out that it is surprising that agreement is found for our measured spectrum for 0–20 ms with the theoretical model at $t = 0.1 \text{ s}$, rather than $t = 1 \text{ s}$, as one might have expected simply by scaling our time against the theoretical time (i.e., our time intervals 0–20, 40–60, and 80–100 ms should scale approximately with $t = 1, 6, \text{ and } 10$ rather than $t = 0.1, 6, \text{ and } 10 \text{ s}$). This notable discrepancy should be addressed in forthcoming experiments and theoretical studies by focusing more closely on the very early phase of the ionization process. A possible explanation for this situation may be that the theoretical spectrum is calculated at a discrete time value, whereas the experimental data is integrated over the first 20 ms time interval. Another possibility is that the calculated

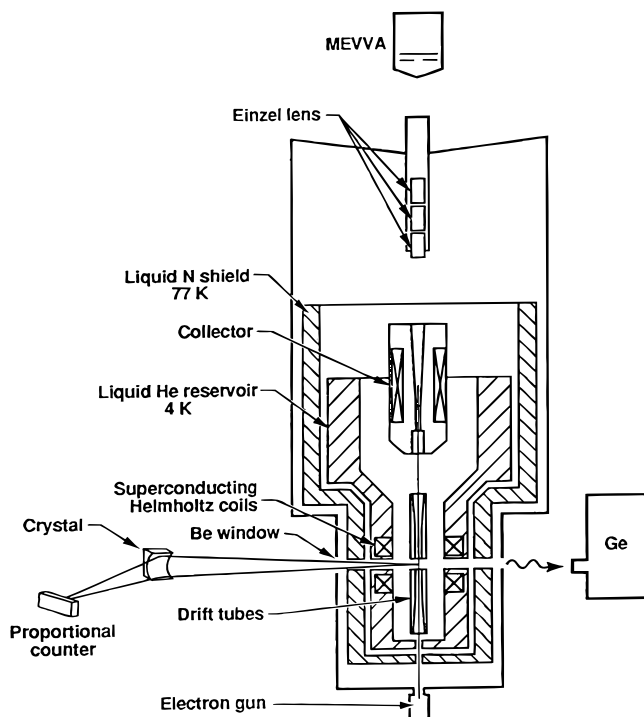


FIG. 1.—Layout of the electron beam ion trap

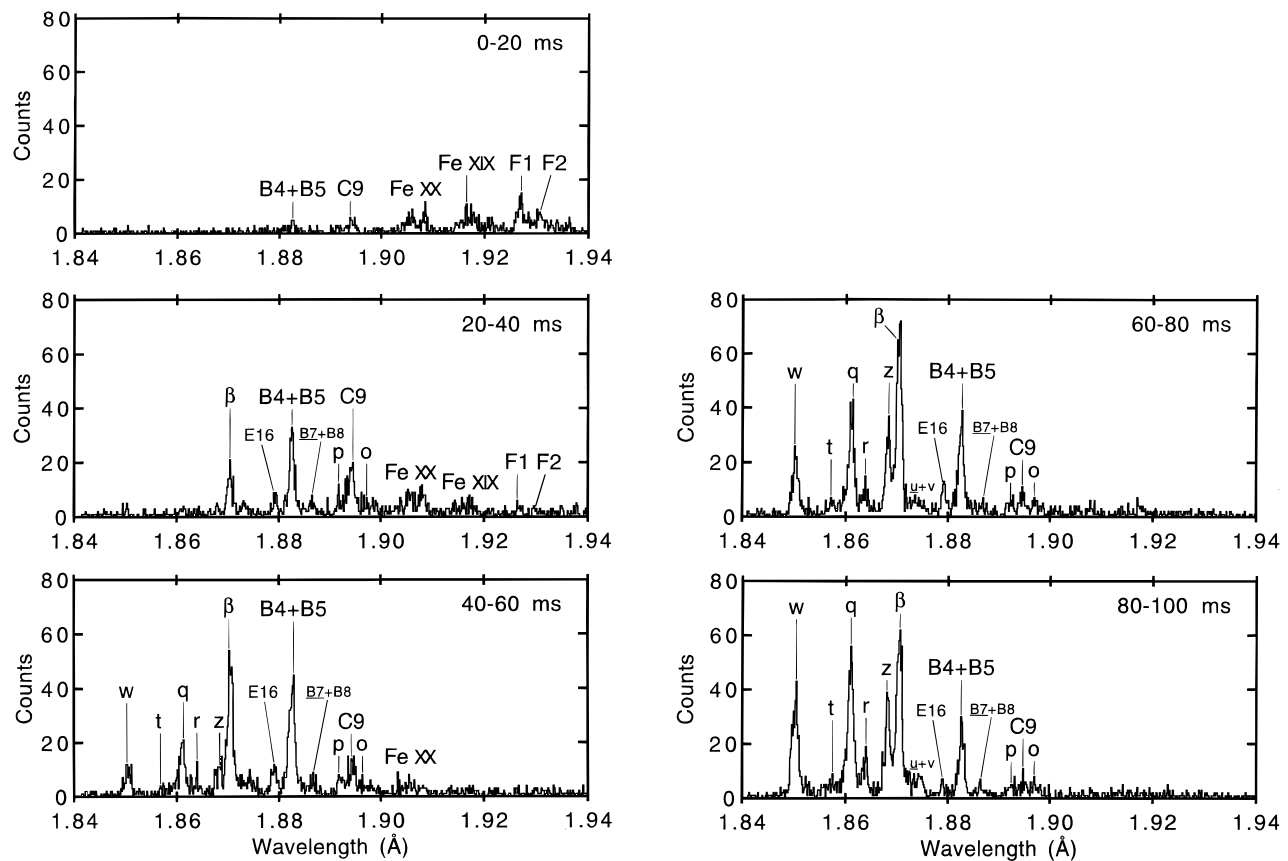


FIG. 2.—K-shell spectra of iron in the region 1.84–1.94 Å measured from the EBIT at an electron beam energy of 12 keV. The data were recorded under transient ionization conditions; presented here are the first five spectra, each recorded for a duration of 20 ms after the injection of iron into the trap at $t = 0$.

intensity of the Fe xx lines may be overestimated at $t = 1$ s; indeed, as we just pointed out above, the lines N5 and N11 dominate the theoretical spectra at $t = 1$ s and $t = 2$ s, whereas they are always weak in our measurements.

The agreement between our results in the interval 0–20 ms and the predictions of Mewe & Schrijver's model at $t = 0.1$ s is illustrated by a comparison between the F1 and F2 lines in Fe xviii, as well as between the Fe xix and Fe xx structures, which are clearly identifiable in both the theoretical predictions and the experimental spectra and have approximately equal intensity ratios. Both the theoretical and the experimental spectra also show a weak feature arising from the line C9 in Fe xxi. Weak emission from the B4 + B5 complex can also be seen in both the theoretical

and experimental spectra, but, as mentioned above, this emission is found to be stronger in the experimental data.

For the higher charge states, Fe xxii–xxv, we find that our spectral data in the interval 40–60 ms closely matches the results obtained from the model at $t = 6$ s. One can observe very similar ratios for the spectral lines designated by w, q, z, β , and E16. However, some discrepancies are found for the emission from Fe xxii. For this ion, the model underestimates the emission from B4 + B5, while the intensity of the B7 + B8 complex appears to be overestimated.

Finally, good agreement is found between our results from 80–100 ms and the model at $t = 10$ s, where the w, q, z, and β lines are dominant in the spectra. As seen previously, there are discrepancies for the emission from Fe xxii. These discrepancies may be in part attributable to small differences in the line positions, which can have an important effect in the detailed structure of the spectral profile. These discrepancies may also be the result of an overestimate of the excitation cross sections in the model of Mewe & Schrijver (1980) or the use of incorrect values for the fluorescent yields.

4. DEPENDENCE ON THE ELECTRON DISTRIBUTION

The shape of the electron distribution plays an important role in the determination of the detailed structure of the observed spectra because inner-shell ionization, which has a threshold energy occurring between 7.1 keV (in Fe i) and 8.7 keV (in Fe xxiv), is an important line-formation process. In fact, the K-shell ionization cross sections are of the same order of magnitude as those for collisional excitation. In the

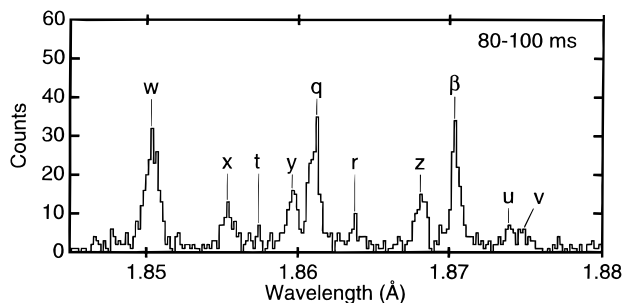


FIG. 3.—K-shell spectrum of iron in the region 1.845–1.880 Å measured from the EBIT under transient ionization conditions at an electron beam energy of 6.9 keV, below the threshold for K-shell ionization, in the time interval 80–100 ms after injection of iron into the trap at $t = 0$.

TABLE 1

LINE IDENTIFICATION, THEORETICAL COLLISIONAL EXCITATION, AND K-SHELL IONIZATION INTENSITY RATES FOR IRON K α FEATURES OF Fe XVIII–XXV

Lines Label	Transition	λ_{exp}	λ_{theo}^a	I_{exc}	I_{ion}
w	$1s^2 \ ^1S_0 - 1s_{1/2} 2p_{3/2} \ ^1P_1$	1.85040	...	3.86	0.00
x	$1s^2 \ ^1S_0 - 1s_{1/2} 2p_{3/2} \ ^3P_2$	1.85532	...	0.39	0.00
t	$1s^2 2s_{1/2} \ ^2S_{1/2} - 1s_{1/2} 2s_{1/2} 2p_{3/2} \ ^2P_{1/2}$	1.85708	1.8572	0.41	0.00
y	$1s^2 \ ^1S_0 - 1s_{1/2} 2p_{1/2} \ ^3P_1$	1.85953	...	0.69	0.00
q	$1s^2 2s_{1/2} \ ^2S_{1/2} - 1s_{1/2} 2s_{1/2} 2p_{3/2} \ ^2P_{3/2}$	1.86101	1.8609	2.57	0.00
r	$1s^2 2s_{1/2} \ ^2S_{1/2} - 1s_{1/2} 2s_{1/2} 2p_{1/2} \ ^2P_{1/2}$	1.86372	1.8638	0.71	0.00
z	$1s^2 \ ^1S_0 - 1s_{1/2} 2s_{1/2} \ ^3S_1$	1.86815	...	1.29	1.32
E3 (β)	$1s^2 2s^2 \ ^1S_0 - 1s_{1/2} 2s^2 2p_{3/2} \ ^1P_1$	1.87041	1.8705	3.07	0.00
u	$1s^2 2s_{1/2} \ ^2S_{1/2} - 1s_{1/2} 2s_{1/2} 2p_{1/2} \ ^4P_{3/2}$	1.87383	1.8735	0.08	0.00
v	$1s^2 2s_{1/2} \ ^2S_{1/2} - 1s_{1/2} 2s_{1/2} 2p_{1/2} \ ^4P_{1/2}$	1.87478	1.8749	0.01	0.00
E16	$1s^2 2s^2 \ ^1S_0 - 1s_{1/2} 2s^2 2p_{1/2} \ ^3P_1$	1.87926	1.8793	0.07	0.31
B3	$1s^2 2s^2 2p_{3/2} \ ^2P_{3/2} - 1s_{1/2} 2s^2 2p_{3/2} \ ^2P_{3/2}$	<1.88262>	1.8817	0.04	0.00
B4	$1s^2 2s^2 2p_{1/2} \ ^2P_{1/2} - 1s_{1/2} 2s^2 2p_{1/2} 2p_{3/2} \ ^2P_{1/2}$	<1.88262>	1.8825	0.98	0.00
B5	$1s^2 2s^2 2p_{1/2} \ ^2P_{1/2} - 1s_{1/2} 2s^2 2p_{1/2} 2p_{3/2} \ ^2D_{3/2}$	<1.88262>	1.8827	0.86	0.00
B7	$1s^2 2s^2 2p_{3/2} \ ^2P_{3/2} - 1s_{1/2} 2s^2 2p_{1/2} 2p_{3/2} \ ^2P_{1/2}$	<1.88664>	1.8869	0.23	0.00
B8	$1s^2 2s^2 2p_{3/2} \ ^2P_{3/2} - 1s_{1/2} 2s^2 2p_{1/2} 2p_{3/2} \ ^2D_{3/2}$	<1.88664>	1.8871	0.10	0.00
B10	$1s^2 2s^2 2p_{1/2} \ ^2P_{1/2} - 1s_{1/2} 2s^2 2p_{1/2} \ ^4P_{1/2}$	<1.89206>	1.8920	0.01	0.27
p	$1s^2 2p_{1/2} \ ^2P_{1/2} - 1s_{1/2} 2s^2 \ ^2S_{1/2}$	<1.89206>	1.8924	0.00	0.10
C7	$1s^2 2s^2 2p_{1/2} 2p_{3/2} \ ^3P_1 - 1s_{1/2} 2s^2 2p_{1/2} 2p_{3/2} \ ^3S_1$	1.89339	1.8934	0.14	0.00
C9	$1s^2 2s^2 2p_{1/2} \ ^3P_0 - 1s_{1/2} 2s^2 2p_{1/2} 2p_{3/2} \ ^3D_1$	<1.89450>	1.8945	1.06	0.38
C10	$1s^2 2s^2 2p_{1/2} 2p_{3/2} \ ^3P_2 - 1s_{1/2} 2s^2 2p_{1/2} 2p_{3/2} \ ^3S_1$	<1.89450>	1.8950	0.06	0.00
o	$1s^2 2p_{3/2} \ ^2P_{3/2} - 1s_{1/2} 2s^2 \ ^2S_{1/2}$	1.89664	1.8969	0.00	0.10
C15	$1s^2 2s^2 2p_{1/2} 2p_{3/2} \ ^3P_2 - 1s_{1/2} 2s^2 2p_{1/2} 2p_{3/2} \ ^3D_1$	1.89862	1.8988	0.21	0.07
C20	$1s^2 2s^2 2p_{3/2} \ ^1D_2 - 1s_{1/2} 2s^2 2p_{1/2} 2p_{3/2} \ ^3D_1$	1.90355	1.9034	0.02	0.01
N4	$1s^2 2s^2 2p_{1/2} 2p_{3/2} \ ^4S_{3/2} - 1s_{1/2} 2s^2 2p_{1/2} 2p_{3/2} \ ^4P_{1/2}$	<1.90477>	1.9042	0.12	0.11
N5	$1s^2 2s^2 2p_{1/2} 2p_{3/2} \ ^4S_{3/2} - 1s_{1/2} 2s^2 2p_{1/2} 2p_{3/2} \ ^2P_{3/2}$	<1.90477>	1.9050	0.27	0.23
N7	$1s^2 2s^2 2p_{1/2} 2p_{3/2} \ ^2D_{3/2} - 1s_{1/2} 2s^2 2p_{1/2} 2p_{3/2} \ ^2D_{3/2}$	1.90536	1.9053	0.01	0.28
N9	$1s^2 2s^2 2p_{1/2} 2p_{3/2} \ ^2D_{5/2} - 1s_{1/2} 2s^2 2p_{1/2} 2p_{3/2} \ ^2D_{3/2}$	1.90634	1.9067	0.00	0.05
N11	$1s^2 2s^2 2p_{1/2} 2p_{3/2} \ ^4S_{3/2} - 1s_{1/2} 2s^2 2p_{1/2} 2p_{3/2} \ ^4P_{5/2}$	1.90824	1.9077	0.30	0.29
N13a	$1s^2 2s^2 2p_{1/2} 2p_{3/2} \ ^2D_{3/2} - 1s_{1/2} 2s^2 2p_{1/2} 2p_{3/2} \ ^4P_{3/2}$	1.91081	1.9100	0.01	0.01
N14a	$1s^2 2s^2 2p_{1/2} 2p_{3/2} \ ^2D_{5/2} - 1s_{1/2} 2s^2 2p_{1/2} 2p_{3/2} \ ^4P_{3/2}$	1.91163	1.9114	0.02	0.01
N14b	$1s^2 2s^2 2p_{1/2} 2p_{3/2} \ ^2D_{3/2} - 1s_{1/2} 2s^2 2p_{1/2} 2p_{3/2} \ ^4P_{5/2}$	<1.91312>	1.9127	0.02	0.02
N15	$1s^2 2s^2 2p_{1/2} 2p_{3/2} \ ^2D_{5/2} - 1s_{1/2} 2s^2 2p_{1/2} 2p_{3/2} \ ^4P_{5/2}$	<1.91312>	1.9140	0.03	0.03
O1	$1s^2 2s^2 2p_{1/2} 2p_{3/2} \ ^3P_2 - 1s_{1/2} 2s^2 2p_{1/2} 2p_{3/2} \ ^3P_1$	<1.91489>	1.9144	0.08	0.17
O3	$1s^2 2s^2 2p_{1/2} 2p_{3/2} \ ^1D_2 - 1s_{1/2} 2s^2 2p_{1/2} 2p_{3/2} \ ^1P_1$	<1.91489>	1.9149	0.01	0.00
O4	$1s^2 2s^2 2p_{1/2} 2p_{3/2} \ ^3P_2 - 1s_{1/2} 2s^2 2p_{1/2} 2p_{3/2} \ ^3P_2$	<1.91733>	1.9164	0.21	0.39
O5	$1s^2 2s^2 2p_{1/2} 2p_{3/2} \ ^3P_0 - 1s_{1/2} 2s^2 2p_{1/2} 2p_{3/2} \ ^3P_1$	<1.91733>	1.9173	0.05	0.22
O6	$1s^2 2s^2 2p_{1/2} 2p_{3/2} \ ^3P_1 - 1s_{1/2} 2s^2 2p_{1/2} 2p_{3/2} \ ^3P_1$	<1.91733>	1.9177	0.03	0.07
O7	$1s^2 2s^2 2p_{1/2} 2p_{3/2} \ ^3P_1 - 1s_{1/2} 2s^2 2p_{1/2} 2p_{3/2} \ ^3P_2$	<1.92046>	1.9197	0.08	0.14
O8	$1s^2 2s^2 2p_{1/2} 2p_{3/2} \ ^1D_2 - 1s_{1/2} 2s^2 2p_{1/2} 2p_{3/2} \ ^3P_1$	<1.92046>	1.9206	0.01	0.03
O10	$1s^2 2s^2 2p_{1/2} 2p_{3/2} \ ^1D_2 - 1s_{1/2} 2s^2 2p_{1/2} 2p_{3/2} \ ^3P_2$	1.92290	1.9226	0.02	0.04
F1	$1s^2 2s^2 2p_{1/2} 2p_{3/2} \ ^2P_{3/2} - 1s_{1/2} 2s^2 2p_{1/2} 2p_{3/2} \ ^2S_{1/2}$	1.92679	1.9258	0.17	0.68
F2	$1s^2 2s^2 2p_{1/2} 2p_{3/2} \ ^2P_{1/2} - 1s_{1/2} 2s^2 2p_{1/2} 2p_{3/2} \ ^2S_{1/2}$	1.93070	1.9297	0.08	0.34

NOTE.—The rate coefficients for excitation (I_{exc}) and ionization (I_{ion}) are given in units of $10^{-12} \text{ cm}^3 \text{ s}^{-1}$, and are calculated for an electron beam energy of 12 keV, as discussed in the text. Measured (λ_{exp}) and calculated (λ_{theo}) wavelengths are in units of Å; values in angle brackets denote blends.

^a From Jacobs et al. (1989), with a shift of +2 mÅ.

higher charge states of iron (Fe xxii–xxv), the effects of K-shell ionization are readily identifiable from an analysis of the intensities of a particular set of lines: z in Fe xxv, E16, in Fe xxiii, o and p in Fe xxiv, and B10 in Fe xxii (see Table 1). Figures 2 and 3 show data taken above and below the K-shell ionization threshold, respectively. Note that in Figure 2 the intensity of line z is comparable with that of the resonance line w, whereas it is less than $\frac{1}{2}$ of the resonance-line intensity in Figure 3. We also find that the Fe xxv intercombination lines x and y are present in the data taken at 6.9 keV, while these lines are too weak to be identifiable in the data taken at 12 keV. This effect occurs because the collisional excitation cross section for the triplet lines (x, y, and z) decreases rapidly as the energy increases. Since x and y have no K-shell ionization contribution (in the low-density limit) to compensate for this decrease, they disappear at high energy, as opposed to z. Consequently, the line-intensity ratio $I(z)/I(x+y)$ can provide a reliable indicator for K-shell ionization in nonequilibrium plasmas.

A similar effect is observed in Fe xxiii. Note that the line E16 is not observed in Figure 3, but is readily detected in Figure 2. This strong enhancement in the intensity of E16 from K-shell ionization occurs because the ground fine-structure state of Fe xxii is $1s^2 2s^2 2p_{1/2} \ ^2P_{1/2}$. The result of K-shell ionization is the formation of the $1s_{1/2} 2s^2 2p_{1/2}$ electronic configuration of Fe xxiii. Of the two possible fine-structure levels, 3P_0 and 3P_1 , only the latter has an allowed radiative decay to the ground level $1s^2 2s^2 \ ^1S_0$, to which is connected by means of a $\Delta J = 1$ transition, resulting in the line E16. Similarly, line z results from the K-shell ionization of the ground state $1s^2 2s_{1/2} \ ^2S_{1/2}$ in Fe xxiv, leading to the excited $1s_{1/2} 2s_{1/2}$ electronic configuration in Fe xxv. Here again there are two levels with such a configuration, 1S_0 and 3S_1 ; the former can decay only by means of a two-photon emission, and thus does not result in an identifiable line, while the latter corresponds to line z.

K-shell ionization also accounts for most of the intensity of the two lines o and p in Fe xxiv because the intensity of

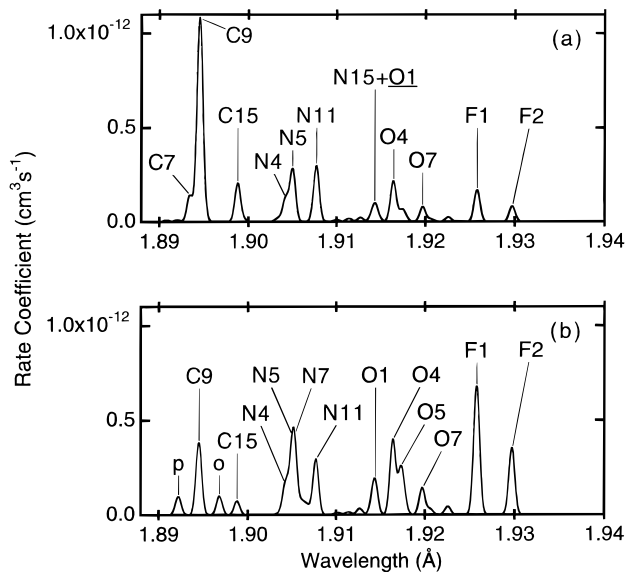


FIG. 4.—Model spectra for the emission from Fe xviii–xxi, in the wavelength range 1.89–1.94 Å. The model has been constructed in the low-density limit, assuming all charge states of iron are initially in the ground state. The two relevant excitation processes are shown separately: (a) collisional excitation, and (b) K-shell ionization. The rate coefficients have been calculated assuming equal populations of the four charge states contributing to the spectra.

the line emission produced by collisional excitation is small compared to that from ionization. The fact that o and p are relatively weak in the observed spectra is due to the small branching ratio for the radiative decay of the $1s2s^2$ upper level. This level undergoes radiative decay only 5% of the time; 95% of the time it decays through autoionization. Line p is also blended with the Fe xxii feature B10, which has an appreciable K-shell ionization intensity as well (see Table 1).

Unlike the higher charge states, the charge states from Fe xviii through Fe xxii do not have lines that are obvious markers for K-shell ionization because collisional excitation can effectively compete with inner-shell ionization in producing any of the observed lines. This fact is apparent from Table 1, where we list the relative line intensities due to the individual K-shell excitation and K-shell ionization processes. This analysis is based on calculations for the collisional excitation rates and radiative branching ratios, as well as the use of semiempirical ionization cross sections from Lodz (1968). The collisional excitation rates have been evaluated in a low-density approximation discussed by Jacobs et al. (1989), in which all ions are assumed to be in the lowest possible fine-structure level. The line-intensity data from Table 1 are displayed in Figure 4, which shows the iron $K\alpha$ emission from 1.89 to 1.94 Å for the two individual line-formation processes. Comparing the two theoretical spectra, we find that the spectral line shape within each charge state is very similar and that both line-formation processes have similar transition-rate coefficients.

5. DETERMINATION OF THE IONIZATION TIME

In order to characterize the early time evolution of the intermediate charge states (Fe xviii–xxii) and determine the ionization time $\eta = N_e t$, we have measured the K-shell

emission in the wavelength range 1.885–1.940 Å with a 7 ms time resolution. The results, which were obtained at an electron beam energy of 12 keV, are shown in Figure 5. For the determination of η from these spectral data, it is necessary to employ a detailed modeling of both the spectral line emission and the time-dependent charge-state balance, as described below.

In our model for the spectral line emission, we have utilized the collisional excitation rates, branching ratios, and K-shell ionization rates employed in the calculation of the individual spectral contributions shown in Figure 4. The results of the complete time-dependent model are presented in Figure 6. These theoretical spectra were obtained by adjusting the relative charge-state population fractions in order to obtain the best fit to our experimental data (Fig. 5). Note that we have introduced an adjustment of the collisional excitation intensity of line C9 in Fe xxii. This adjustment was necessary because the intensity of this line is overestimated by our adoption of the simplified low electron density approximation, in which it is assumed that only the lowest fine-structure level of each ion is populated. Using a more detailed collisional-radiative determination for the population densities of the individual levels, Lemen et al. (1986) have shown that this approximation is not sufficiently accurate for Fe xxii in the density range of our experiments. An adjusted line intensity has been determined by a consideration of the variation, within the density range $N_e = 10^{11}$ – 10^{13} cm^{-3} , of the corresponding line intensity obtained from the model of Lemen et al. (1986). The adjustment was by approximately a factor of 2.

A comparison of the theoretical and experimental spectra shows good agreement for all spectral features. The charge-state population fractions required to obtain this agreement are presented in Table 2. We have constructed a time-dependent model for the evolution of the charge-state balance that incorporates ionization cross sections from Lotz (1968) and radiative recombination cross sections from Kim & Pratt (1983). The characteristic timescale for the ionization process is determined by η , as illustrated in Figure 7. Since the time t is known in our experiment, we varied the electron density in our calculation. The resulting values for the charge-state population fractions corresponding to different values of the density N_e were compared with those of Table 2. In particular, we considered the sum of the squares of the differences plotted in Figure 8 for values of the electron density in the range $(1\text{--}3) \times 10^{12}$ cm^{-3} . Density values outside this range were also considered but yielded poor fits to the data. Figure 8 shows that the best agreement is found for $N_e = 1.7 \pm 0.3 \times 10^{12}$ cm^{-3} . For comparison, an estimate of the true density in the trap can be derived

TABLE 2
CHARGE-STATE FRACTION DETERMINED FROM A FIT OF SYNTHETIC SPECTRA TO OBSERVED SPECTRA

Time Interval (ms)	Fe xvii	Fe xviii	Fe xix	Fe xx	Fe xxii
0–7	17	8	4	1	0
7–14	10	8	5	3	0
14–21	10	25	10	7	5
21–28	4	19	22	8	5
28–35	0	0	3	9	7

NOTE.—Results are given as a percentage of the total iron population.

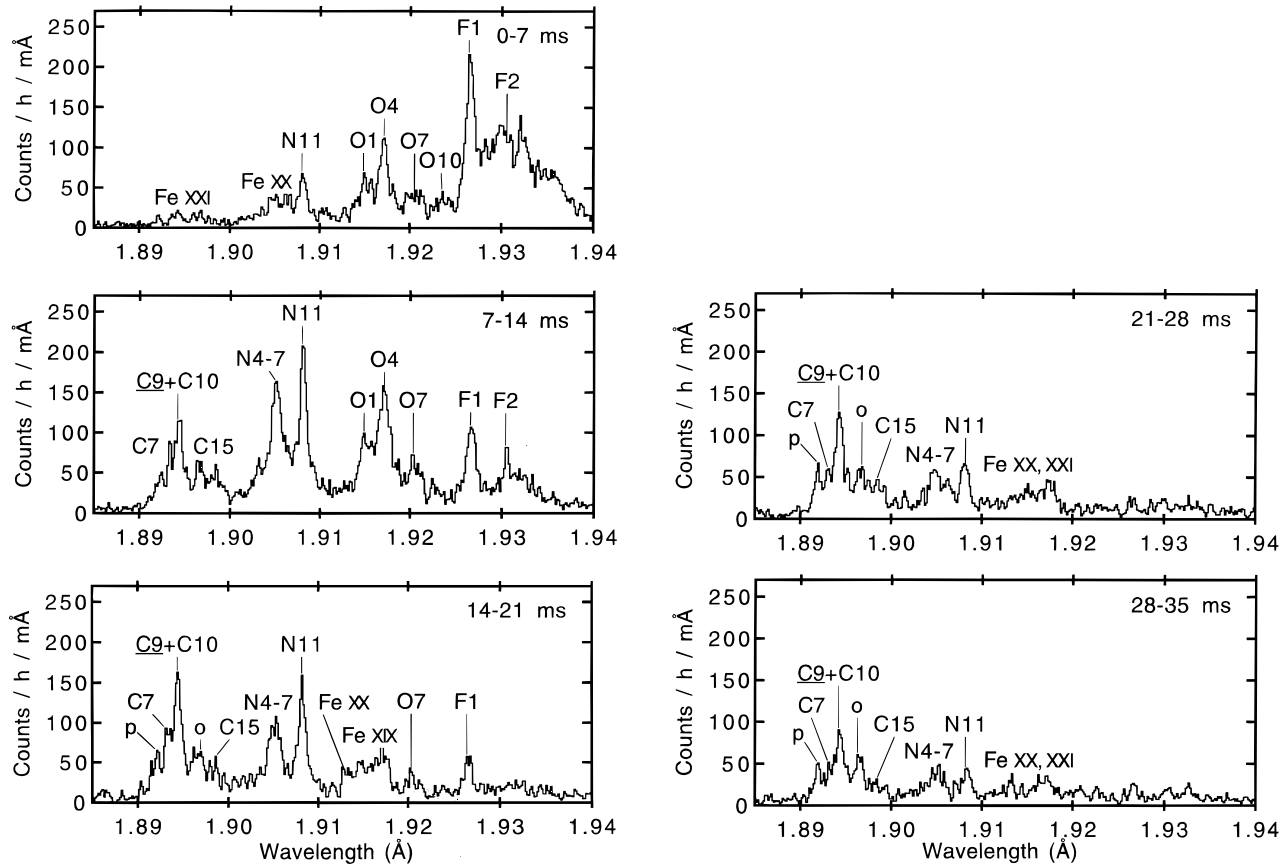


FIG. 5.—K-shell spectra of iron in the region 1.885–1.94 Å measured from the EBIT under transient ionization conditions at an electron beam energy of 12 keV. Presented here are the first five spectra recorded for a duration of 7 ms after injection of iron into the trap.

from the known beam current density J (5300 A cm^{-2}) and beam energy E (12 keV) using the formula

$$N_e = \frac{J}{e\sqrt{2E/m_e}}, \quad (1)$$

where e and m_e denote the electron charge and mass, respectively. This formula yields a value for N_e of $5.1 \times 10^{12} \text{ cm}^{-3}$; however, ions in the trap oscillate in and out of the electron beam, so that the effective electron density they see is lower; the value depends on the experimental conditions. For experimental conditions similar to those used for the present measurement, the ion temperature was shown to be about 700 eV (Beiersdorfer et al. 1995), which, according to Levine et al. (1988), means that the ions spend only about a third of their time inside the electron beam. Taking this effect into account, the effective electron density becomes about $1.5 \times 10^{12} \text{ cm}^{-3}$, in good agreement with our spectroscopically derived value. The accuracy of the data in Table 2 determines the uncertainty in the sum of the squared differences (error bars in Fig. 8) and thus the uncertainty of the inferred value of the density N_e . Even with the use of our simple ionization model, a single value of the electron density was sufficient to describe our experimental data to an accuracy of about 20%. In other words, this simple ionization model enables one to realistically predict the charge-state population fractions as functions of the ionization time η to an accuracy of 20%. A determination of

η with similar precision should be possible in the investigation of nonequilibrium astrophysical plasmas.

6. CONCLUSION

We have presented the results of high-resolution measurements of the K α emission of iron, from Fe xviii to Fe xxv, obtained under well-controlled and well-diagnosed laboratory conditions in a low-density environment, using a transient ionization technique that allows the simulation of conditions that are believed to exist in nonequilibrium astrophysical plasmas. Spectral signatures for the fundamental atomic line formation mechanisms have been identified, and the importance of the shape of the ionization continuum has been demonstrated. Our experimental results provide agreement with many of the theoretical predictions of Mewe & Schrijver (1980) on ionizing plasmas. From our data, we have been able to infer the time evolution of the charge-state population fractions for Fe xvii–xxi. By comparing the measured population fractions with the results obtained from theoretical simulations, we have been able to determine, within a precision of 20%, the ionization time $\eta = N_e t$. High-resolution spectral measurements of the iron K-shell emission from supernova remnants hold a promise of a determination of η within a similar precision. Such measurements are useful for understanding the thermal history of the shocked gas and for unambiguous determinations of the electron density and the line-of-sight extent of the emitting filaments.

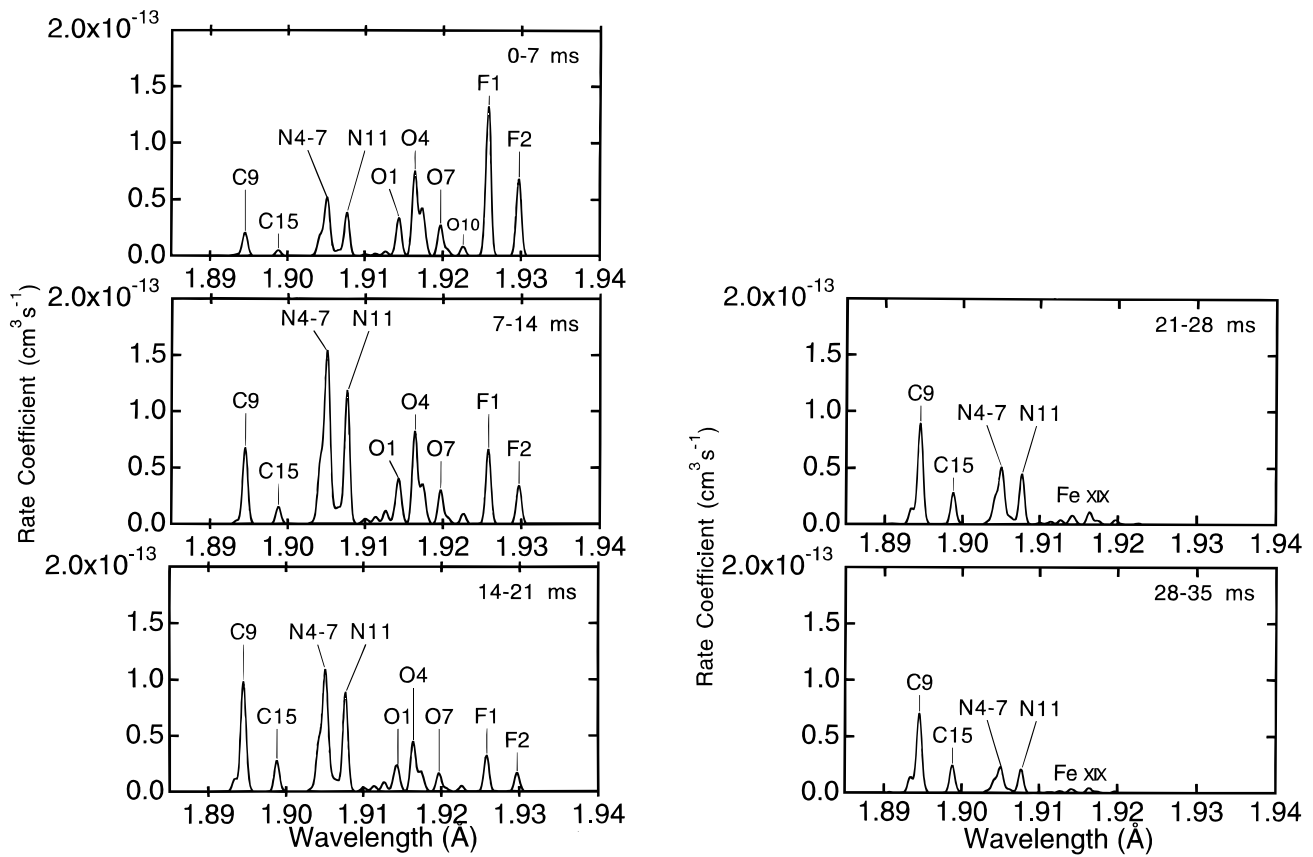


FIG. 6.—Time-dependent synthetic spectra showing the emission from Fe xviii–xxi in the wavelength range 1.85–1.94 Å. The spectral model incorporates the contributions from collisional excitation and K-shell ionization, together with charge-state population fractions determined to give the best fit to the experimental data shown in Fig. 5.

This work was supported by NASA’s X-Ray Astronomy Research and Analysis Program under grant NAGW-4185 and was performed under the auspices of the US Department of Energy by the Lawrence Livermore National

Laboratory under contract no. W-7405-ENG-48. The work of V. L. J. has been supported by the US Department of Energy under contract DE-AI02-93-ER54198 to the Naval Research Laboratory.

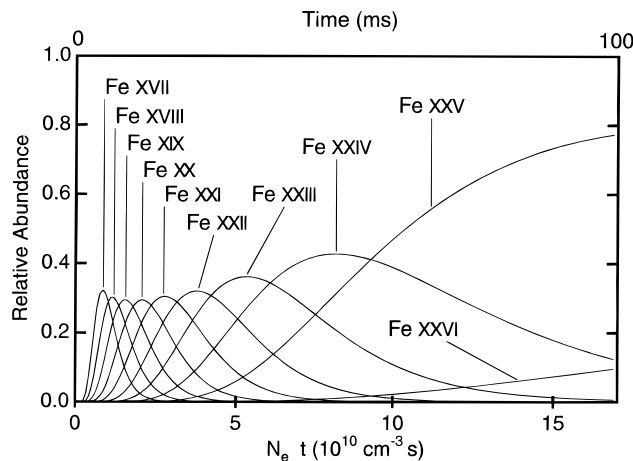


FIG. 7.—Relative abundances of the Fe xvii through Fe xxvi charge states as functions of the ionization parameter $\eta = N_e t$ for an electron beam energy of 12 keV. The upper horizontal scale shows the time elapsed from the beginning of the ionization process, assuming an electron density $N_e = 1.7 \times 10^{12} \text{ cm}^{-3}$.

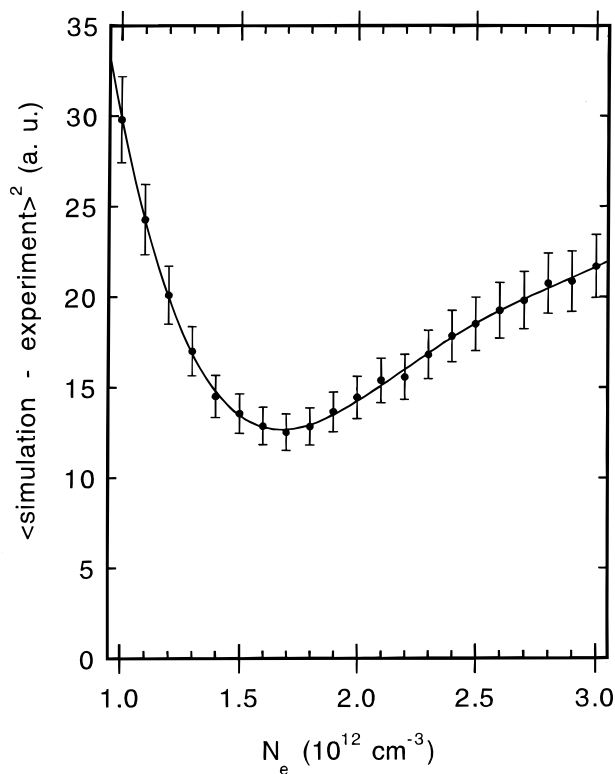


FIG. 8.—Sum of the squared differences between the calculated and measured charge-state population fractions as a function of the assumed electron density.

REFERENCES

- Beiersdorfer, P., et al. 1993a, in *UV and X-Ray Spectroscopy of Astrophysical and Laboratory Plasmas*, ed. E. H. Silver & S. M. Kahn (Cambridge: Cambridge Univ. Press), 59
- Beiersdorfer, P., Decaux, V., Elliott, S., Widman, K., & Wong, K. 1995, *Rev. Sci. Instrum.*, **66**, 303
- Beiersdorfer, P., et al. 1990, *Rev. Sci. Instrum.*, **61**, 2338
- Beiersdorfer, P., Phillips, T., Jacobs, V. L., Hill, K. W., Bitter, M., von Goeler, S., & Kahn, S. M. 1993b, *ApJ*, **409**, 846
- Brown, I. G., Galvin, J. E., MacGill, R. A., & Wright, R. T. 1986, *Appl. Phys. Lett.*, **49**, 1019
- Decaux, V., & Beiersdorfer, P. 1993, *Phys. Scr.*, **T47**, 80
- Decaux, V., Beiersdorfer, P., Osterheld, A., Chen, M., & Kahn, S. M. 1995, *ApJ*, **443**, 464
- Itoh, H. 1977, *PASJ*, **29**, 813
- . 1978, *PASJ*, **30**, 489
- Jacobs, V. L., Doschek, G. A., Seely, J. F., & Cowan, R. D. 1989, *Phys. Rev. A*, **39**, 2411
- Kafatos, M. C., & Tucker, W. H. 1972, *ApJ*, **175**, 837
- Kim, Y. S., & Pratt, R. H. 1983, *Phys. Rev. A*, **27**, 2913
- Lemen, J. R., Phillips, K. J. H., Doschek, G. A., & Cowan, R. D. 1986, *J. Appl. Phys.*, **60**, 1960
- Levine, M. A., Marrs, R. E., Henderson, J. R., Knapp, D. A., & Schneider, M. B. 1988, *Phys. Scr.*, **T22**, 157
- Lotz, W. 1968, *Z. Phys.*, **216**, 241
- Marrs, R. E., Levine, M. A., Knapp, D. A., & Henderson, J. R. 1988, *Phys. Rev. Lett.*, **60**, 1715
- Mewe, R., & Schrijver, J. 1975, *Ap&SS*, **38**, 345
- . 1978, *A&A*, **65**, 115
- . 1980, *A&A*, **87**, 261
- Shapiro, P. R., & Knight, J. W. 1978, *ApJ*, **224**, 1028
- Shapiro, P. R., & Moore, R. T. 1976, *ApJ*, **207**, 460
- . 1977, *ApJ*, **217**, 621
- Silver, E. H., & Kahn, S. M., eds. 1993, *UV and X-Ray Spectroscopy of Astrophysical and Laboratory Plasmas* (Cambridge: Cambridge Univ. Press)
- Treves, A., Perola, G. C., & Stella, L. eds. 1991, *Iron Line Diagnostics in X-Ray Sources*, *Lecture Notes in Physics*, **385** (Berlin: Springer-Verlag)
- von Hámos, L. 1933, *Ann. Phys.*, **17**, 716